Research Article ISSN 2694-5614

Journal of Pharmaceutical Research and Development

H_2 Production From Wastewaters Containing Sulphur via Photocatalysis Using TiO_2-N-GO Nanocomposite

Delia Teresa Sponza

Dokuz Eylül University, Engineering Faculty, Environmental Engineering Department Buca, İzmir TURKEY

***Correspondence author**
Delia Teresa Sponza
Dokuz Eylül University
Engineering Faculty
Environmental Engineering Department Buca
İzmir TURKEY

Submitted : 29 June 2023 ; Published : 24 July 2023

Citation : Delia Teresa Sponza (2023). H_2 Production From Wastewaters Containing Sulphur via Photocatalysis Using TiO_2-N-GO Nanocomposite. J Pharma Res Dev., 4(2): 1-10. DOI : https://doi.org/10.47485/2694-5614.1019

Abstract

In this study, nitrogen containing TiO_2 nanoparticles were doped on GO and TiO_2-N-GO nanocomposite was produced under laboratory conditions to treat the chemical industry wastewater containing high H_2S under UV light. 1%- 1%-3%, 3%- 1%-1% and 1%- /15%-1%3 ratios for TiO_2-N-GO nanocomposite composition was researched for maximal hydrogen production. The structural, optical and morphological aspects of nanocomposites were studied using XRD, UV-DRS, Raman, XPS, FESEM, and TEM. The TiO_2-N-GO nanocomposite with 2% GO, exhibited enhanced photocatalytic H_2 production 3450 µmol h^{-1} under 60 min UV light irradiation The increase of photocatalytic activity was the high N doping resulting in high porous surface in the nanocomposite.

Keywords : GO, TiO_2-N-GO, chemical industry, wastewater, H_2S, H_2 production.

Introduction

Among various kinds of energy resources, hydrogen is one of the potential green energy sources because of its eco-friendliness, high energy combustion, and carbon-free emission (Han et al., 2012). Recently, the solar-drivable photocatalytic water-splitting technique has emerged as a prominent way to produce hydrogen from wastewater (Khan et al., 2002). In general, the semiconductive photocatalysts show the outstanding activity of photocatalytic water-splitting; however, the photo-corrosion and the fast photocarrier recombination have restricted their tangible application for photocatalytic hydrogen production (Maeda et al., 2006). To overcome this issue, many types of strategies have been proposed; for example, the incorporation of various dopants into carbon-based materials, noble metals, and non-metals as well as the formation of co-catalysts with homo- and hetero-structures using transition-metal oxides (TMOs) (Zou et al., 2004). To achieve a higher hydrogen-production efficiency, fabricating the high-quality TMO-based semiconductive photocatalysts is essential. Particularly, a higher photo-stability and a higher photo-response to visible light are desired to increase the photocatalytic hydrogen-production efficiency. Considering such criteria, titanium dioxide (TiO_2) can be an excellent candidate for photocatalysts because of its high photo-stability, high conductivity, high surface area, chemical inertness, non-toxicity, huge abundance, and low cost (Hu et al., 2013). On the other hand, the high bandgap energy (3.2 eV) and the low reaction kinetics would somewhat hinder the photocatalytic water-splitting performances.

To utilize solar energy effectively, many attempts have been made to modify the properties of TiO_2, such as doping with transition metal ions (Yang et al., 2012) or nonmetal anions (Meng et al., 2013), and sensitization with organic dyes (Jia et al., 2011). Among the nonmetal-doping TiO_2 photocatalysts, the simplest and most feasible TiO_2 modification approaches for achieving visible-light-driven photocatalysis seem to be N-doping, that is, doping nitrogen atoms into interstitial (or substitutional) sites in the crystal structure of TiO_2. To date, little research has been conducted on gaining in-depth information on the properties of the substitutional N-doped TiO_2, as well as its photocatalytic activity. Different dopants result in TiO_2 of different properties and consequently alter the photocatalytic activity of the materials. Currently, few works have focused on the synergistic effects of nitrogen dopant and calcination temperature on the characteristics and visible-light-induced photoactivity of N-doped TiO_2 (Jia et al., 2011).

Accordingly, for efficient use of solar energy in photocatalytic reactions, it is important to extend the TiO_2 optical response into the visible light region (Peng et al., 2007). Therefore, the fabrication of nitrogen-doped TiO_2(N-TiO_2) of appreciable visible light absorptivity has been considered as a promising approach since the N_2p derived states are generated immediately above the valence band (VB) causing band gap narrowing (Pei et al., 2013). It has been reported that interstitial nitrogen is supposed to have direct influences on the electronic states and light activities rather than substitutional ones (Deng et al., 2011).

Additionally, defect states originated from oxygen vacancies and reduced Ti species ($Ti3^{+}$) in the band gap together with N-derived states are shown to contribute to the light absorption characteristics of N–TiO_2 in the visible light region (Zhang et al., 2011). Lately, a density functional theory has shown that N prefers to replace Ti rather than O to form NOx (Pei et al., 2013). Furthermore, oxygen vacancies near surface regions act as recombination centers and thus weaken the photocatalytic activities. The stability of N-doped TiO_2 is also an important issue of concern since it may be lost during treatments like calcination, solubilization, etc., resulting in decreased catalytic activity. Indeed, oxygen deficiencies and loss of nitrogen are not only affect the N-doped TiO_2 electronics but also influence the fast recombination of electron-hole pairs and thus affect seriously the photocatalytic efficacy. Hence, to prevent the recombination of charge carriers and to extend the light absorption into visible light region, a constructive conductive substrate is urgently required for enhancing the photocatalytic activity. The combination of TiO_2 with carbonaceous materials has attracted researcher attention since it enhances the efficiency of photocatalytic activity (Kuo, 2009). Particularly, graphene of magnificent electrical, mechanical, surface texturing and thermal properties has been incorporated with TiO_2 to form composites of high potential use in photocatalytic applications (Kongsong et al., 2018; Kovalevskiy et al., 2020). Introduction of TiO_2-based nanocomposites with graphene is simultaneously results in superior electron transfer owing to the excellent electrical conductivity of graphene (Chizari et al., 2012). At low loadings, graphene can work as an efficient electron conducting net-work (Ba et al., 2016). Accordingly, modification of TiO_2 nanomaterials with graphene or graphene oxide has shown great interests (Gomes et al., 2019), (Xie et al., 2013), (Yang et al., 2013), (Wang et al., 2009).

These outstanding features attracted graphene to be utilized as a promising support material to disperse and stabilize N-TiO_2 nanoparticles which in turn enhance the photocatalytic hydrogen production by water splitting contaınıng sulphure. Some drawbacks can be effectively released by the hybridization of host photocatalysts (e.g., TiO_2) with highly-conjugated carbonaceous materials (e.g., activated carbon (AC), carbon nanotubes, graphitic carbon, graphene, graphene oxide, reduced graphene oxide, etc.) (Lin et al., 2022; Vu et al., 2021). Among them, graphene oxide nanostructures provide a strong interfacial interaction in between the photocatalyst species so that the rapid charge separation occurs and the electron-hole recombination rate decreases. This would eventually improve the hydrogen production efficiency during the photocatalytic wastewater splitting process. Graphene oxide has superior mechanical strength, excellent mobility of charge carriers, high thermal conductivity and large specific surface area. These outstanding features attracted graphene to be utilized as a promising support material to disperse and stabilize N-TiO_2 nanoparticles which in turn enhance the photocatalytic hydrogen production by water splitting containing sulphure.

Accordingly, loading TiO_2 nanocrystallites on major amounts of graphene or graphene oxide nanosheets will not improve the photocatalytic efficiency but indeed will increase the adsorption capability, which is not the issue and indeed not required. Increasing graphene nanosheet concentration is going to enlarge its aggregation around TiO_2 low contents affecting the latter good orientation towards light absorption and thus decreases the photoactivity. Due to the high oxygen functionality of graphene oxide, the interaction with N-TiO_2 is permitted for high wet-ability, disperse-ability and for obtaining both continuous and consistent nanophotocatalysts stable against light for longer time(Meiling et al., 2020; Lin-Wei et al., 2019).

Sulfide ions present in industrial wastes either as S2- or hydrogen sulfide (H_2S) are toxic having an unpleasant odor. Petrochemical industry releases H2S containing (15–20%) wastewater as a by-product, and their treatment process produces elemental sulfur. Also, sewage treatment plant releases the wastewater containing sulphide ion with concentration greater than 1200 mg/L. At present a large amount of energy being spent for this treatment, whereas photocatalytic process can be effectively utilized to recover H_2 gas (Keishi et al., 2019; Minxue et al., 2019).

The nitrogen-doping of graphene will also change the affinity of graphene to hydrogen donor via hydrogen bond produced by nitrogen lone pair electrons, which is very useful for photocatalytic hydrogen production by water-splitting reaction. Owing to the effective impact of these factors on the electronic property and chemical reactivity of graphene, nitrogen-doped graphene (N-graphene) has been applied to synthesize the semiconductor nanocomposites as photocatalysts for hydrogen evolution, such as molybdenum disulfide/n-type nitrogen-doped reduced graphene oxide (Muhammad Aniq Shazni et al., 2019) and nitrogen-doped graphene/CdS (Chen-Chen et al., 2018).

In order comprehensively to explore the effect of nitrogen-doping on the photocatalytic efficiency of semiconductor nanocomposite of TiO_2 and graphene, N-TiO_2/GO- is synthesized herein as photocatalysts for hydrogen production through the in-situ nitrogen-doping of TiO_2 while the TiO_2/N-GO nanocomposite is prepared. The effects of the nitrogen content and the ratio of GO on the hydrogen production from sulphure present in the chemical industry were investigated. The effects of temperature, Ph and photooxidation times on the H2 productions were researched and the reusability properties of the N-TiO_2/GO nanocomposite was analysed.

Material and Methods

Synthesis of nitrogen-doped graphene oxide

The mixture of lithium nitride (2.5 g) and tetrachloromethane (60 mL) was treated with ultrasonic dispersion for 20 min. Then the mixture was transferred into a 100-mL stainless steel autoclave and repeatedly deaerated by N_2. The reaction was carried out at 25^0 C for 10 h in nitrogen atmosphere. The product was washed sequentially with 10wt%HCl aqueous solution, distilled water, ethanol and freezedried. The resulting product was denoted as N-graphene.Samples using different

$TiCl_4$:urea ratios i.e. 35 1:2, 1:4 and 1:6 (w/w) were prepared .The N-TiO_2 was prepared by heat treating homogeneous 0.05 mole TiCl4 and 0.2 mole urea (1:4 w/w of $TiCl_4$:urea) solution in absolute ethanol at 150°C to obtained an intermediate product (Ti-urea complex) which was further annealed at 300°C, 400°C and 500° 40 C for 3h. The productannealed at 300°C is named as T_2.GO (with 2% loading) in absolute ethanol (without urea) at 150° 45°C to obtained the intermediate product which was further annealed at 300°C for 3h and denoted as T3. The other products with dopants and graphene composites with 0.5%,1% and 2% loading of GO were annealed at 300°C for 3h and denoted as T_4, T_5 and T_6, respectively.

These products were then subjected to XRD, UV-DRS, Raman, XPS, FTIR, FESEM, TEM and BET analysis for their characterization.

Photodecomposition of H_2S

The cylindrical quartz photochemical reactor was filled with 200 ml 0.25 M aqueous KOH and purged with argon for 1 h.Hydrogen sulphide (H_2S) containing chemical industry wastewater was bubbled through the solution for about 1h at the rate of 2.5 ml min−1 at 299 K. Undoped TiO_2, NTiO_2, TiO_2 /GO and N-TiO_2 60 /GO (0.2 g) was introduced into the reactor and irradiated with a solar lightThe escaped hydrogen sulfide was trapped in a NaOH solution. The amount of hydrogen gas was measured with Hatch Lange device. The evolved hydrogen was then analyzed for its purity using a gas chromatograph (Model Shimadzu GC-14B, MS-5 Å column. All the samples were tested for their catalytic activity under identical conditions for a continuous period of of increasing minutes (30, 60 and 200 min).

Characterization

The crystalline phases and the crystallite size of the photocatalyst was identified using an X-ray powder diffraction (XRD) with Cu Kα irradiation. The optical properties of the powder samples were studied using an UV-visible-near infrared spectrometer. Room temperature micro Raman scattering (RS) was performed using a HR 800-Raman 80 Spectroscopy, France, with an excitation at 632.81 nm by a coherent He–Ne ion laser and a liquid nitrogen cooled CCD camera to collect and process the scattered data. The nature of chemical bonds formed in N-TiO_2 and GO were examined using X-ray photoelectron spectroscopy with a base pressure greater than 1.0×10^{-9} Pa and Mg Kα FTIR spectra's were recorded with a spectrometer. The Brunauer-Emmett-Teller (BET) specific surface area (SBET) of the powders was analyzed by nitrogen adsorption apparatus.

Results and Discussion

XRD analysis Results

The peaks observed at 26.1o , 39.9o , 49.0o , 57.2o , 63.8o , 70.3o and 79.0o 30 are indexed as (102), (005), (202), (213), (206), (221) and (217) respectively(Figure1). This ındicetes the formation of anatase crystalline structure. No peaks were observed for carbon species in the T3-T6 samples due to low amount of graphene. The observations indicates that the full width at half maximum is more for the anatase peaks of N-TiO_2 (T_2) which is attributed to the doping of nitrogen into the TiO_2 nanocomposite. In T3-T6 samples , the presence of increasing amount of graphene increase the degree of crystallization.

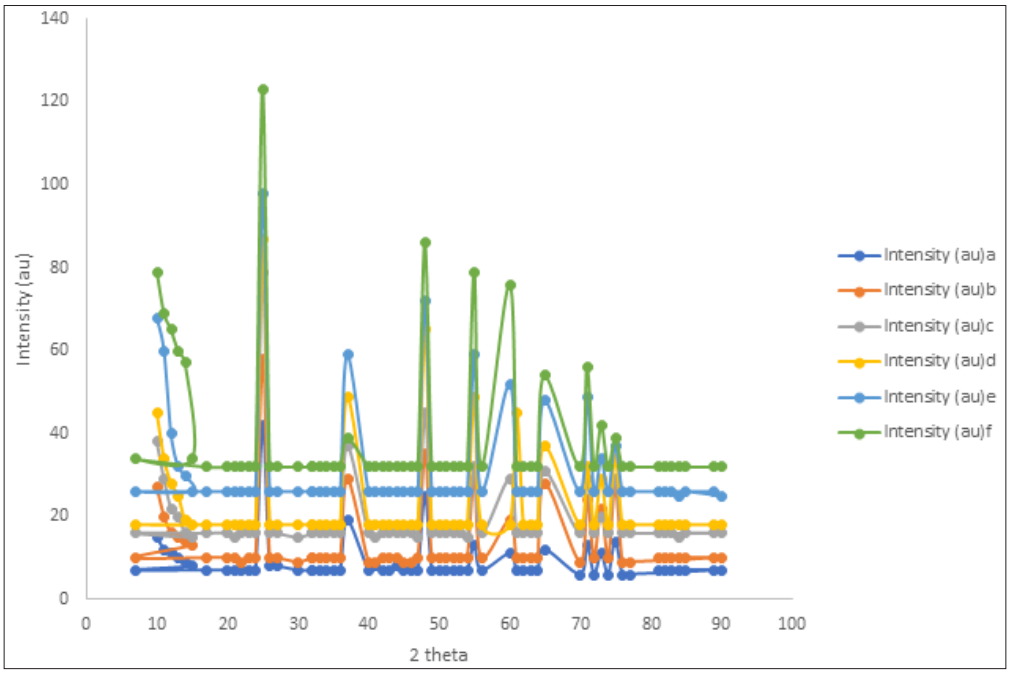

Figure 1 : XRD analysis in (a) undoped TiO_2 (T_1), (b) N-TiO_2 (T_2) (c) TiO_2 loading with 2% GO (T_3), N-TiO_2 loading with 0.5% GO (d) N-TiO_2 loading loading with 0.8% GO (T_4), (e) N-TiO_2 loading with 1% GO (T_5) and N-TiO_2 loading with 25 % GO (f) (T6)

UV-Vis diffuse reflectance spectra of TiO_2 solely(T1), N-TiO_2, (T2), iO_2/GO(T3), N-TiO_2-GO(T4-T6) nanocomposites

The spectra shows the absorption edge at 389 nm (3.18 eV) for undoped TiO_2 (T_1) as commonly observed for anatase TiO_2. The band gap energies of samples T_2-T_6 were determined to be 2.95 (424 nm), 2.58 (477 nm), 2.58 (486 nm), 2.55 (492 nm), 2.43 (517 nm) eV, respectively (Figure 2).

The extended visible light absorption edge was observed with increasing the graphene content in composite samples. It is obvious that N-TiO_2 /GO shows much stronger absorption of visible light than TiO_2 /GO nanocomposite. When N was doped into TiO_2 60 /GO nanocomposite, the absorption edge of T_6 sample is extended to 518 nm (2.43eV).

Figure 2 : UV-DRS spectra of (a) undoped TiO_2 samples (T_1) (b) N-TiO_2 (T_2) (c) TiO_2 containing 2% GO (T_3). N-TiO_2-containing 0.5% GO (d) (T_4), (e) N-TiO2-containing 1 % GO (T_5) , N-TiO_2-containing 2 % GO (f) (T_6)

Raman Spectrum

The comparison of the Raman spectra of undoped TiO_2 (T1), N-TiO_2 (T2), TiO_2/GO (T3) and N-TiO_2 /GO (T4-T6) samples showed that GO Raman spectrum shows two typical bands located at 1329 and 1595 cm−1. These correspond to disordered sp2 carbon and well ordered graphite carbon structures, respectively.Undoped TiO_2 (T1), exhibited several characteristic bands at 142, 394, 513, and 637 cm−1. These can be corresponded with Eg (1), B1g(1), A1g+B1g(2) and Eg(2) modes of anatase, respectively. N-TiO_2 (T2), TiO_2 /GO (T3) and N-TiO_2 /G0 (T4-T6) exhibited similarities with Raman bands mentioned for anatase. T3-T6 samples , exhibited Raman spectrum at D (1329 cm^{-1}) and G (1611 cm^{-1}) bands of graphene, indicating incorporation of GO in the all other nanocomposites.

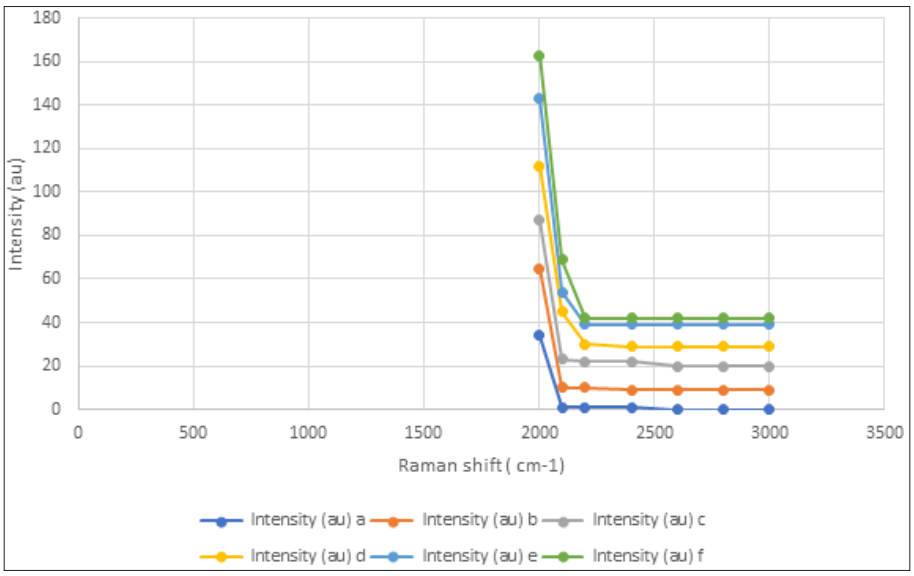

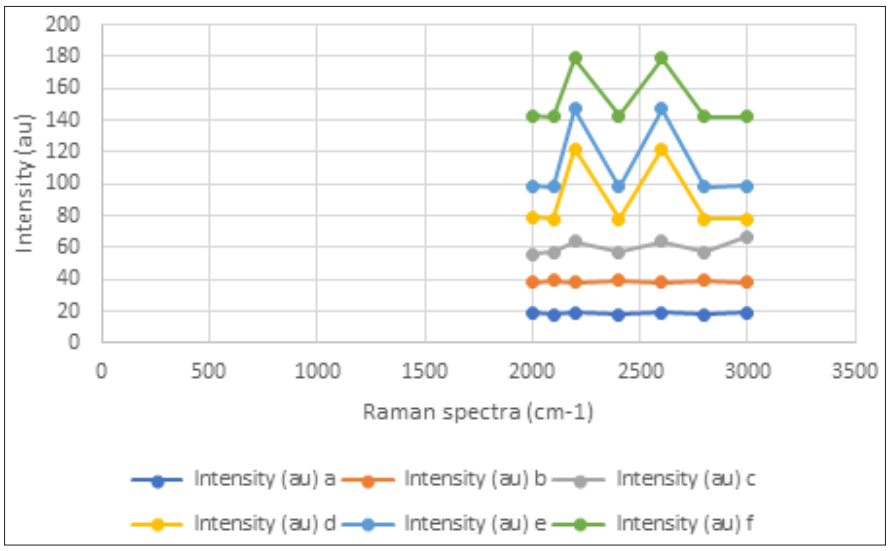

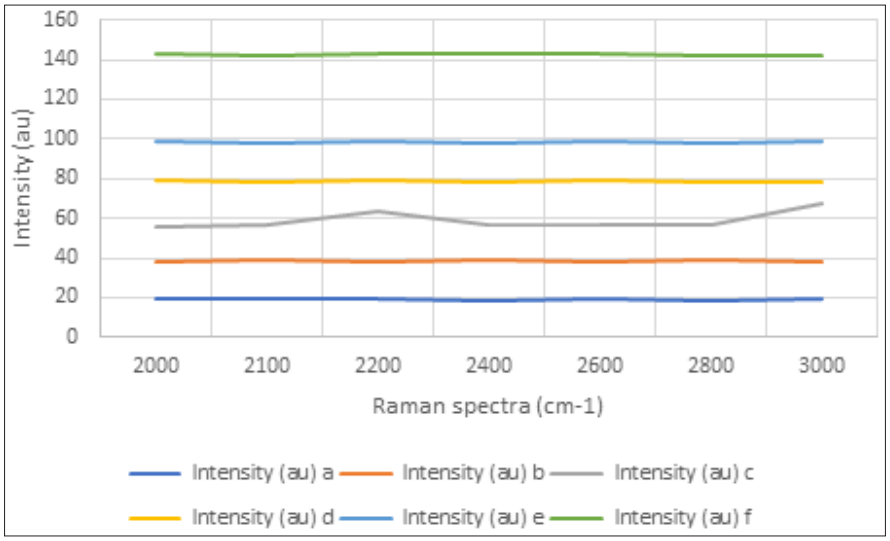

Figure 3(A, B, C) : Raman spectrum of samples (a) undoped TiO_2 (T1) (b) N-TiO_2 (T2) (c) TiO_2 with 2% GO (T3), N-TiO_2 with 0.5% GO(d) (T4), (e) N-TiO_2 with 1.0% GO (T5), (f) N-TiO_2 with 2.0% GO (T6). (B) shows the magnified range from 1004-2004 cm-1 (C) shows the magnified range from 2004-3004 cm-1

Fig. 3(A) shows a comparison of the Raman spectra of undoped TiO_2 (T1), N-TiO_2 (T2), TiO_2 /GO (T3) and N-TiO_2 /GO (T4-T6) nanocomposites).

For GO , Raman spectrum shows two typical bands located at 1328 and 1595 cm−1. These were correlated to sp2 carbon (D-band) and graphite carbon structures (G-band), respectively. Undoped TiO_2 (T1), exbibited bands at 143, 395, 515, and 638 cm−1. Thsese can be attributed to the Eg (1), B1g(1), A1g+B1g(2) and Eg(2) modes of anatase, respectively. N-TiO_2 (T2), TiO_2 /GO (T3) and N-TiO_2 /GO (T4-T6) nanocomposites, exhibited Raman bands for anatase. The Raman spectrums in T3-T6 samples exhibited the D (1327 cm-1) and G (1606 cm-130) bands of GO, indicating the incorporation of graphene in the aforementioned nano composites.Fig. 3(B) shows the Raman spectrum of all nanocomposites exclusively in the range of 1103-2003 cm-1. It was observed two dominated peaks centered at about 1327 cm-1 (D band) and 1607 cm-1 (G band) exhibiting the presence of graphene in the nanocomposites containing GO.The G band for samples (T3-T6) is broadened and red shifted to 1605 cm-1 after the reduction of GO (1593 cm-1). This can be explained by Ti-O-C bond formation which exhibits a close interaction between TiO_2 and GO and impoving a strong integration across the interface between GO and anatase TiO_2. Fig. 3(C) shows the Raman spectrum of the undoped TiO2 (T1), N-TiO_2 (T2), TiO_2 /GO (T3) and N-TiO_2 / G0 (T4-T6) nanocomposites in the range of 2003-3003 cm-1 . 2D peak is not observed in the expanded range. The increasing number of layers of graphene, 2D peak becomes broader and less intense. The elevated D/G intensity ratio as compared to that of GO is an indicator of the presence of GO.

X-ray photoelectron spectroscopy (XPS) measurement results

In order to investigate the chemical changes occurred on the surface of the nanocomposite formation by during detection of the signals of N, Ti, O and C to elucidate the interaction between graphene, TiO_2 and N-TiO_2 nanocomposites. Fig. 4 shows the high resolution XPS spectra for C (1s), N (1s), O (1s) and Ti (2P) core levels of the N-TiO_2 /GO nanocomposite. The XPS spectrum of C1S from GO is deconvoluted into three peaks which are ascribed to the following functional groups: Sp2 bonded carbon (C-C, 285.6 eV), epoxyl/hydroxyls (C-O, 288 eV), carbonyls (C=O, 286.9 eV)(data not shown). The first peak indicates the presence of 2D carbon structure, the latter two peaks indicate the presence of high percentage of oxygen-containing functional groups. The XPS spectrum of C(1s) from N-TiO_2 /GO shows that the peak intensity for oxygen containing functional groups substantially lowered as compared to the intensity for oxygen containing functional groups in the spectrum of GO(Fig. 4a). the band located at 283.6 eV can be assigned to the presence of the Ti-C bond. These bands exhibited the peak deconvolution of the Ti(2p) core level, as investigated in the Fig. 4 b shows the N(1s) core level spectrum where the peak at 399.7 eV can be attributed to the anionic N in O-Ti-N linkage while a peaks at 402.3 and 402.6 eV are ascribed to the molecularly chemisorbed γ-N2 and N-Ox surface speciesrespectively. These peaks clearly indicate that nitrogen was substitutionally doped into TiO_2 lattice. Fig. 4 c shows O(1s) narrow scan spectrum. The peaks around 531.9 eV and 533.1 eV are attributed to the Ti-O-Ti i.e. lattice oxygen andTi-OH adsorbed on the sample surface, respectively.Fig. 4d shows core level photoelectron spectrum, the peaks located at 459.2 eV and 466.1 eV are assigned to Ti (2p3/2) and Ti (2p1/2), respectively. The presence of small amount of hydrophilic groups on the surface of GO, such as hydroxyl and carboxyl groups, can enhance the photocatalytic activity. Since GO are excellent electron 60 acceptors, the Ti-C and Ti-O-C bonds can act as effective channels in electron transferring from the photoexcited N-TiO_2.

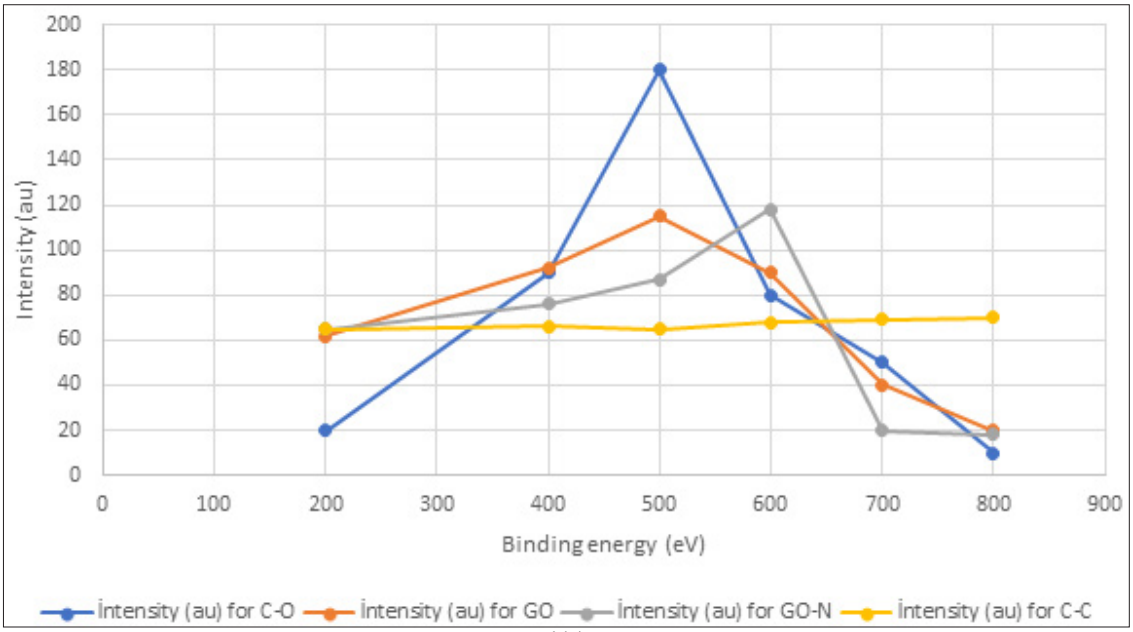

4(a)

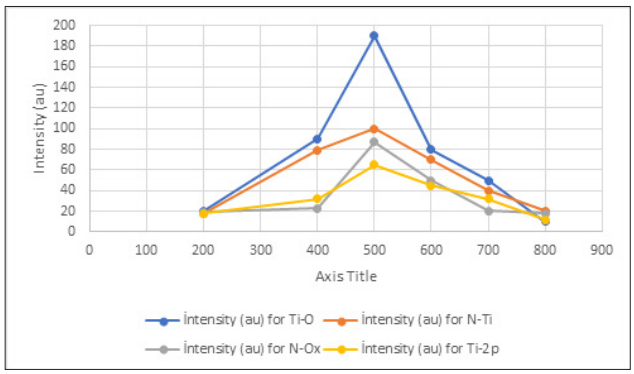

4(b)

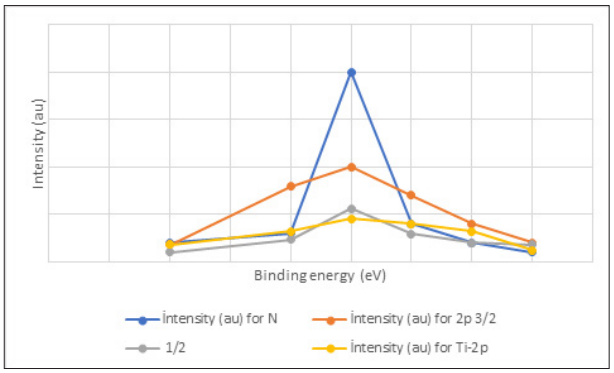

4(c)

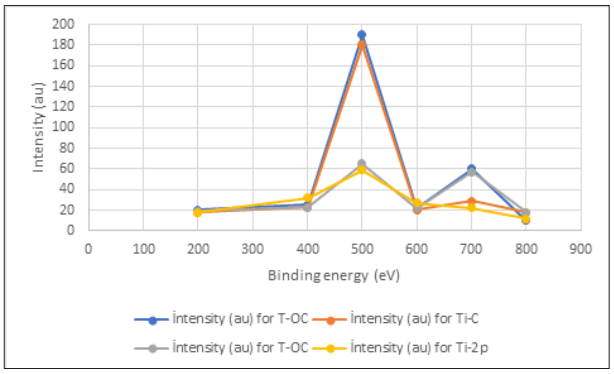

4(d)

Figure 4 : XPS patterns of N-TiO_2 with 2% GO loading (T6) (a) C(1_s), (b) N(1_s), (c) O(1_s), (d)Ti(2_p).

FTIR spectra

The GO displayed several characteristic absorption bands of oxygen containing groups(Fig. 5 A). The IR absorption at 1727 cm-1 could be attributed to the C=O stretching vibration. The peak at around 964 cm-1, 1057 cm-1 , 1252 cm-1 orresponds to the epoxy stretching, alkoxy C-O stretching and C-O-C stretching peaks, respectively. The broad band at 1562 cm-1 can be assigned to in-plane vibrations of aromatic C=C Sp2 hybridized carbons. As against the evidencce of these oxygen-containing groups of GO, the absence small intensity of bands of oxygen containing functional groups (C-O, C-O-C) in samples (T3-T6) was noteworthy (Fig. 5B). T1 and T2 samples show pressnce of sharp Ti-O-Ti bands in their IR studies at 652 cm-1. Oxygen containing groups mentioned above must have reacted with the species which are in close contact with GO, namely Ti. However, the broadening of Ti-O-Ti peak suggests the presence of a peak due to Ti-O-C bond. Thus, Ti-O-Ti bonding is well understood.

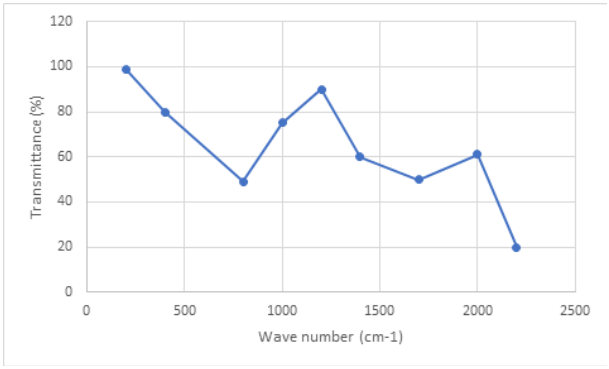

5(A)

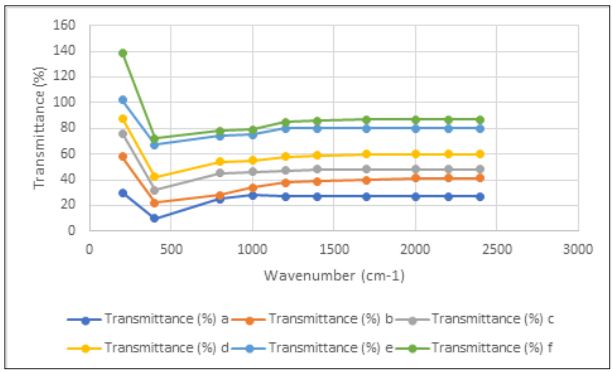

5(B)

Figure 5(A, B): FTIR spectra of samples (A) GO, (B) (a) undoped TiO_2 (T1) (b) N-TiO_2 (T2) (c) TiO_2 with 2% GO (T3), N-TiO_2 with 0.5% GO (d) (T4), (e) N-TiO_2 with 1% GO 1% (T5), N-TiO_2 with 2% GO (f) (T6).

H2 production from H2S

Table 1 shows the hydrogen production from the photodecomposition of H2S using undoped TiO_2 (T1), N-TiO_2 (T2), TiO_2/GO (T3) and N-TiO_2 /GO (T4-T6). Control researches indicated no significant hydrogen production was detected in the absence of irradiation or photocatalyst samples. This showed that hydrogen is produced only through photocatalytic reaction. Undoped TiO_2 shows low hydrogen production compared to the other nanocomposites. N-TiO_2 Containing 2% GO exhibited the highest hydrogen production of 8976 mol/min during 60 min photooxidation. N-TiO2 containinh no GO exhibited a hydrogen production of rate of around 3470 mol /min. This can be attributed to N doping in TiO_2 enhances hydrogen evolution rate. By incorporating of GO at a ratio of 2% to N-TiO_2 elevated the hydrogen production 3 times compared to undoped TiO_2. As a result hydrogen production increased by increase of GO percentage.Hydrogen evolution increases with increasing graphene content (see Table 1). However, further increasing the amount of graphene affects the hydrogen production which is unfavorable beyond 2%. The active sites of N-TiO_2 may not covered fully by 2% GO. Indeed, This GO ratio was not lead to shielding of the active sites on the nanocatalyst surface and also did not decrease the intensity of light through the depth of the reaction solution.

Sample properties	S -BET (micronmeter)	H2 production mol/ min
Undoped TiO_2	98	2340
N-TiO_2 with no GO	103	3470
TiO_2 with 0.1% GO	134	4500
N-TiO_2 with 0.5% GO	208	6987
N-TiO_2 with 1% GO	221	7897
N-TiO_2 with 2% GO	243	8976

Table 1 : BET and H2 Productions in different types of nanocomposite compositions

Effects of Ni/TiO_2/ GO Ratios and pH variations on H2 production rate

The maximum H2 yields was detected at high GO ratios as 12300 mol/min at pH=7 (Table 2).The GO in the nanocomposite is as an electron acceptor and transporter. GO has been reported to be competitive candidate as an acceptor material due to its π-conjugation structure and has excellent mobility of charge carriers and large specific surface area. Therefore, rapid transport of charge carriers could be achieved and an effective charge separation consequently accomplished. Overall, both the electron accepting and transporting properties of graphene in the nanocomposite could contribute to the enhancement of photocatalytic activity. Additionally, as per the PL study, the lower intensity peaks observed in graphene doped samples indicating that the electron-hole recombination on the surface of catalysts is largely inhibited to generate more free photoelectrons and holes. Hence, the enhanced photocatalytic activity of N/TiO2 / GO nanocomposite with a ratio of 1/1/3 is mainly attributed to more effective charge transportation and separation arisen from the strong chemical bonding of N-TiO_2 and GO.

Sample properties	S -BET (micronmeter)	H2 production mol/ min		
		pH		
		4	7	10
N/TiO_2/GO =3/1/1	223	3200	3200	4000
N/TiO_2 /GO= 1/3/1	229	5437	9752	6900
N/TiO_2 / GO =1/1/3	259	7654	12300	8760

Table 2: Variatios of H2 production rates versus Ni/TiO_2/ GO ratios and pH

The H2 production from H2S under visible-light irradiation with N/TiO_2 / GO nanocomposite are as follows:

$H_2S + OH^- \longleftrightarrow HS^- + H_2O$ (1)

N/TiO_2 / GO nanocomposite $\longleftrightarrow$ N-TiO_2 (h^+) + GO (e^-) (2)

Oxidation $2HS^- + N\text{-}TiO_2 (2h^+) \longleftrightarrow 2S + 2H^-$ (3)

Reduction $2H^- + GO (2e^-) \longleftrightarrow H_2$ (4)

Transport of electrons from TiO_2 to GO is energetically a favorable process. Thus, efficiently separation of photo-induced charge carriers leads to lowering of charge recombination and effectively enhance the photocatalytic performance. These electrons are accessible to the adsorbed H+ ions to form H2. Therefore, the synergistic effect of H2 production on catalyst surface is because of extended visible light absorption due to 'N' doping, optimal GO ratio and efficient charge separation by photocatalytic H2S splitting to H2 with suitable TiO_2/ N / GO nanocatalyst ratios.

Effects of increasing temperatures and photooxidation times oon H2 production rate

Table 3a and 3b shows the H2 productions versus increasing temperatures and photooxidation times at different nanocomposite components. The effectiveness of N/TiO_2 / GO nanocatalyst was evaluated by investigating the effect of temperature at different contact times on H2 production. H2 production increases with temperature because reforming and decomposition reactions; both are very endothermic reactions; as a result, a small increase in temperature results in a significant increase in H2 production. The hydrogen concentration increases from 7698 mol/ min up to 12987 mol/min oas the temperature was increased from 18o C to 31oC. Increasing of temperature to 41 Oc did not increase significantly the H2 production significantly.

The product yield increases with photooxidation time. At low photooxidation time such as 30 min the H2 productions was low as the photooxidation time was increased to 60 min the maximum H2 productions was detected. At long photooxidation time the H2 productions lowered.

Sample properties	H2 production mol/ min		
	Temperature (Oc)		
	18	31	45
N/TiO_2/GO =3/1/1	3200	4856	4100
N/TiO_2 /GO= 1/3/1	5499	9752	6986
N/TiO_2 / GO =1/1/3	7698	12987	11760

Table 3 a: Effect of temperature on H2 production

Sample properties	H2 production mol/ min		
	Photooxidation time (min)		
	30	60	200
N/TiO2/GO =3/1/1	3180	4856	4200
N/TiO2 /GO= 1/3/1	5487	9745	6970
N/TiO_2 / GO =1/1/3	7675	12956	11855

Table 3b: Effects of increasing photooxidation time on H2 production rate

Reuse of N/TiO_2 / GO nanocomposite

N/TiO_2 / GO nanocomposite describes its economic behavior and shows the reprocessing capability up to n number of cycles. In the first cycles the H2 production rates was not lowered after 12 000 minutes and 400 cycles while the H2 production was recorded as 11987 mol/min after 2000 min and 660 cycles utilization of the same nanocomposite (Table 4).

Sample properties	H2 production mol/ min
N/TiO_2 / GO =1/1/3 (1,2 mg)	
Photooxidation time (min)	
30	12900
60	12900
120	12900
200	12900
400	12900
800	12900
2000	12900
3000	12879
5000	12879
7000	12879
8000	12879
12000	12879
14000	11989
20000	11989

Table 4 : Recovery of N/TiO_2 / GO nanocomposite

Conclusions

$N/GO/TiO_2$ nanocomposite was produced under laboratory conditions to produce

photocatalyic hydrogen production from H2S. The same nanocomposite was used 660 times for 2000 min with a H2 production of 11987 mol/min after 2000 min and 660 by using 1,2 mg N/TiO_2 / GO nanocomposite with a ratio of 1/1/3. The optimal conditions for maximal H2 production of 12956 mol7MİN were 30 min photooxidation time at pH =7.0 and At a temperature of 31°c.

References

1. Han, Z. J., Qiu, F., Eisenberg, R., Holland, P. L., & Krauss, T. D. (2012). Robust photogeneration of H2 in water using semiconductor nanocrystals and a nickel catalyst. *Science, 338*(6112), 1321-4. DOI: 10.1126/science.1227775
2. Khan, S., Al-Shahry, M., & Ingler, W. B. (2002). Efficient photochemical water splitting by a chemically modified n-TiO_2. *Science, 297*(5590), 2243-5. DOI: 10.1126/science.1075035
3. Maeda, K., Teramura, K., Lu, D. L., Takata, T., Saito, N., Inoue Y., & Domen K. (2006). Photocatalyst releasing hydrogen from water e enhancing catalytic performance holds promise for hydrogen production by water splitting in sunlight. *Nature, 440*((7082), 295. DOI: 10.1038/440295a
4. Zou, Z. G., Ye, J. H., Sayama, K., & Arakawa, H. (2001). Direct splitting of water under visible light irradiation with an oxide semiconductor photocatalyst. *Nature, 414*(6864), 625-7. DOI: 10.1038/414625a
5. Hu, P., Pramana, S. S., Cao, S. W., Ngaw, C. K., Lin, J. D., Loo, S. C. J., & Tan TT. (2013). Ion-induced synthesis of uniform single-crystalline sulphide-based quaternary-alloy hexagonal nanorings for highly efficient photocatalytic hydrogen evolution. *Adv Mater, 25*(18), 2567-72. DOI: 10.1002/adma.201204545
6. Schiros, T., Nordlund, D., Pálová, L., Prezzi, D., Zhao, L., Kim, K. S., Wurstbauer, U., Gutiérrez, C., Delongchamp, D., Jaye, C., Fischer, D., Ogasawara, H., Pettersson, L. G., Reichman, D. R., Kim, P., Hybertsen, M. S., & Pasupathy, A. N. (2012). Connecting dopant bond type with electronic structure in n-doped graphene. *Nano Lett, 2*(8), 4025-31. DOI: 10.1021/nl301409h
7. Meng, F. K., Li, J. T., Cushing, S. K., Zhi, M. J., & Wu, N. Q. (2013). Solar hydrogen generation by nanoscale p-n Junction of p-type molybdenum disulfide/n-type nitrogen-doped reduced graphene oxide. *J Am Chem Soc, 135*, 10286-9. https://doi.org/10.1021/ja404851s
8. Jia, L., Wang, D. H., Huang, Y. X., Xu, A. W., Yu, H. Q. (2011). Highly durable ndoped graphene/CdS nanocomposites with enhanced photocatalytic hydrogen evolution from water under visible light irradiation. *J Phys Chem, 115*(23), 11466-73. DOI:10.1021/jp2023617
9. Peng, F., Cai, L. F., Yu, H., Huang, L., & Wang, H. J. (2007). The solvothermal preparation method of a nitrogen-doped titanium dioxide. ZL 200610122601.5.
10. Pei, F. Y., Liu, Y. L., Xu, S. G., Lu, J., Wang, C. X., & Cao, S. K. (2013). Nanocomposite of graphene oxide with nitrogen-doped TiO2 exhibiting enhanced photocatalytic efficiency for hydrogen evolution. *Int J Hydrogen Energy, 38*(6), 2670-7. DOI:10.1016/j.ijhydene.2012.12.045
11. Deng DH, Pan XL, Yu L, Cui Y, Jiang YP, Qi J, Qiang F., Qikun X., & Xinhe B. (2011). Toward ndoped graphene via solvothermal synthesis. *Chem Mater, 23*(5), 1188-93. DOI:10.1021/cm102666r
12. Zhang, C. H., Fu, L., Liu, N., Liu, M. H., Wang, Y. Y., & Liu, Z. F. (2011). Synthesis of nitrogen-doped graphene using embedded carbon and nitrogen sources. *Adv Mater, 23*(8), 1020-4. DOI: 10.1002/adma.201004110
13. Pei, F. Y., Liu, Y. L., Zhang, L., Wang, S. P., Xu, S. G., & Cao, S. K. (2013). TiO2 nanocomposite with reduced graphene oxide through facile blending and its photocatalytic behavior for hydrogen evolution. Mater Res Bull, 48, 2824-31.
14. Kuo, S. W. (2009). Hydrogen bond-mediated self-assembly and supramolecular structures of diblock copolymer mixtures. *Polym Int, 58*(5), 455-6. DOI:10.1002/pi.2513
15. Kongsong, P., Taleb, A., Masae, M., Jeenarong, A., Hansud, P., & Khumruean, S. (2018). Effect of nitrogen doping on the photocatalytic activity and hydrophobic property of rutile TiO2 nanorods array. *Surface and Interface Analysis, 50*(5), 1271–1277. DOI:10.1002/sia.6518
16. Kovalevskiy, N., Selishchev, D., Svintsitskiy, D., Selishcheva, S., Berezin, A. & Kozlov, D. 2020 Synergistic effect of polychromatic radiation on visible light activity of N-doped TiO2 photocatalyst. *Catalysis Communications 134*, 105841. DOI: 10.1016/j.catcom.2019.105841
17. Chizari, K., Deneuve, A., Ersen, O., Florea, I., Liu, Y., Edouard, D., Janowska, I., Begin, D, & Pham-Huu, C. (2012). Nitrogen-Doped Carbon Nanotubes as a Highly Active Metal-Free Catalyst for Selective Oxidation, *J. Chemsuschem, 5*(1), 102-108.

DOI: 10.1002/cssc.201100276
18. Ba, H., Duong-Viet, C., Liu, Y., Nhut, J. M., Granger, P., Ledoux, M. J., & Cuong, P. H. (2016). Nitrogen-Doped Carbon Nanotube Spheres as Metal-Free Catalysts for the Partial Oxidation of H2S. *Comptes Rendus Chimie, 19*(10), 1303-1309. DOI: 10.1016/j.crci.2015.09.022
19. Gomes, J., Lincho, J., Domingues, E., Quinta-Ferreira, R. M., & Martins, R. C. (2019). N-TiO2 photocatalysts: a review of their characteristics and capacity for emerging contaminants removal. *Water, 11*(2), 373. https://doi.org/10.3390/w11020373
20. Xie, G. C, Zhang, K., Guo, B. D., Liu, Q., Fang, L., & Gong, J. R. (2013). Graphenebased materials for hydrogen generation from light-driven water splitting. *Adv Mater, 25*(28), 3820-39. DOI: 10.1002/adma.201301207
21. Yang, S., Gong, Y., Zhang, J., Zhan, L., Ma, L., Fang, Z., Vajtai, R., Wang, X. &, Ajayan, P. M. (2013). Exfoliated graphitic carbon nitride nanosheets as efficient catalysts for hydrogen evolution under visible light. *Adv Mater, 25*(17), 2452-6. DOI: 10.1002/adma.201204453
22. Wang, X., Maeda, K., Thomas, A., Takanabe, K., Xin, G., Carlsson, J. M., Domen, K., Antonietti, M. (2009). A metal-free polymeric photocatalyst for hydrogen production from water under visible light. *Nat Mater, 8*(1), 76-80. DOI: 10.1038/nmat2317
23. Lin, J., Bas, V. D., Longfei, W., Clément, M., Jan, P. H., Viorica, T., Marc, T. M. K., Dennis, G. H. H., & Grégory F. S. (2022). Predoped Oxygenated Defects Activate Nitrogen-Doped Graphene for the Oxygen Reduction Reaction. *ACS Catalysis, 12*(1), 173-182. https://doi.org/10.1021/acscatal.1c03662
24. Vu, N., Brian, D. E., Svitlana, P., & Shubham, V. (2021). Periodic Trends behind the Stability of Metal Catalysts Supported on Graphene with Graphitic Nitrogen Defects. *ACS Omega, 6*(42) , 28215-28228. https://doi.org/10.1021/acsomega.1c04306
25. Meiling, F., Xiangchuan, P., Weiran, L., & Haining, Z. (2020). Carbon-Covered Hollow Nitrogen-Doped Carbon Nanoparticles and Nitrogen-Doped Carbon-Covered Hollow Carbon Nanoparticles for Oxygen Reduction. *ACS Applied Nano Materials, 3*(4), 3487-3493. https://doi.org/10.1021/acsanm.0c00222
26. Lin-Wei, C., Lei, T., Hang, N., Sheng-Qi, C., & Hai-Wei, L. (2019). Sub-2 nm Ir Nanoclusters Immobilized on Mesoporous Nitrogen-Doped Carbons as Efficient Catalysts for Selective Hydrogenation. *ACS Applied Nano Materials, 2*(10), 6546-6553. https://doi.org/10.1021/acsanm.9b01471
27. 27. Keishi, A., Seiji, O., & Koichiro, S. (2019). Work Function Lowering of Graphite by Sequential Surface Modifications: Nitrogen and Hydrogen Plasma Treatment. *ACS Omega, 4*(15), 16531-16535. https://doi.org/10.1021/acsomega.9b02208
28. Minxue, H., Shuai, L., Shipeng, G., Pengping, X., Kang, Y., Shi, C., Changlai, W., & Qianwang, C. (2019). Silver Nanoparticles Encapsulated in an N-Doped Porous Carbon Matrix as High-Active Catalysts toward Oxygen Reduction Reaction via Electron Transfer to Outer Graphene Shells. *ACS Sustainable Chemistry & Engineering, 7*(19), 16511-16519. https://doi.org/10.1021/acssuschemeng.9b03736
29. Muhammad Aniq Shazni, M. H., Nur Hamizah, Z. A., Syed, M. H., Poh, C. O., Mohd, I. S., & Abdul, M. H. (2019). Wafer-Scale Fabrication of Nitrogen-Doped Reduced Graphene Oxide with Enhanced Quaternary-N for High-Performance Photodetection. *ACS Applied Materials & Interfaces, 11*(4), 4625-4636. https://doi.org/10.1021/acsami.8b19043
30. Chen-Chen, W., Jin-Tao, R., Zhong-Pan, H., & Zhong-Yong, Y. (2018). Nitrogen-Doped Defect-Rich Graphitic Carbon Nanorings with CoOx Nanoparticles as Highly Efficient Electrocatalyst for Oxygen Electrochemistry. *ACS Sustainable Chemistry & Engineering, 6*(11), 15811-15821. https://doi.org/10.1021/acssuschemeng.8b04406
31. Xinlei, G., Siwei, Y., Jing, Z., Gang, W., Peng, H., Hongrui, S., Haobo, Y., Luting, Y., Guqiao, D., & Yuejin, Z. (2019). Graphite-N Doped Graphene Quantum Dots as Semiconductor Additive in Perovskite Solar Cells. *ACS Applied Materials & Interfaces, 11*(41), 37796-37803. https://doi.org/10.1021/acsami.9b13375